NASA TN D-1007

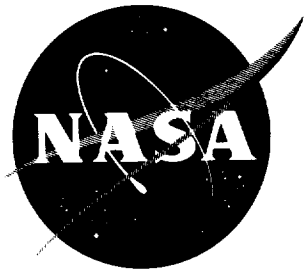

TECHNICAL NOTE

D-1007

INVESTIGATION OF THE LOW-SUBSONIC FLIGHT CHARACTERISTICS OF A MODEL OF A REENTRY VEHICLE WITH A THICK FLAT 75° SWEPT DELTA WING AND A HALF-CONE FUSELAGE

By Peter C. Boisseau

Langley Research Center
Langley Air Force Base, Va.

NATIONAL AERONAUTICS AND SPACE ADMINISTRATION

WASHINGTON February 1962

M

NATIONAL AERONAUTICS AND SPACE ADMINISTRATION

TECHNICAL NOTE D-1007

INVESTIGATION OF THE LOW-SUBSONIC FLIGHT CHARACTERISTICS OF A MODEL OF A REENTRY VEHICLE WITH A THICK FLAT 75° SWEPT DELTA WING AND A HALF-CONE FUSELAGE

By Peter C. Boisseau

SUMMARY

An investigation of the low-subsonic flight characteristics of a model having a thick flat 75° swept delta wing with a half-cone fuselage on the upper surface has been made in the Langley full-scale tunnel over an angle-of-attack range from about 20° to 40°. Static and dynamic force test data were also obtained with the model.

The longitudinal flight characteristics were considered to be generally satisfactory over the angle-of-attack range of the investigation. Because of low damping of the Dutch roll oscillation, the lateral stability and control characteristics were considered to be poor throughout the angle-of-attack range (20° to 30°) where flights were possible without artificial damping. Artificial damping in roll greatly improved the lateral characteristics so that flights could be made up to an angle of attack of about 40°.

INTRODUCTION

An investigation is being conducted by the National Aeronautics and Space Administration to provide information on the stability and control characteristics of some proposed configurations suitable for lifting reentry from satellite orbit over the speed range from hypersonic to low subsonic. (For example, see refs. 1 to 4.) The present investigation was made to provide some information on the longitudinal and lateral stability and control characteristics at low subsonic speeds of a model having a highly swept, flat delta wing with a half-cone fuselage on the upper surface.

The investigation included flight tests in the Langley full-scale tunnel to determine the low-subsonic flight characteristics of the model for an angle-of-attack range from 20° to 40°. Force tests were also made to determine the static and dynamic stability and control characteristics of the model for correlation with flight-test results.

Included in the flight investigation were tests to determine the effect of center-of-gravity location on the longitudinal stability and control characteristics. These tests were made at an angle of attack of 29° with artificial damping in roll added. Also studied in the flight tests was the effect of artificial roll damping on the lateral stability and control characteristics.

SYMBOLS

L
1
8
0
7

The lateral data are referred to the body system of axes, and the longitudinal data are referred to the wind system of axes. (See fig. 1.) All moments are measured about a center-of-gravity position located longitudinally at 30.0 percent of the mean aerodynamic chord.

b	wing span, ft
C_D	drag coefficient, $\frac{F_D}{qS}$
C_L	lift coefficient, $\frac{F_L}{qS}$
C_l	rolling-moment coefficient, $\frac{M_X}{qSb}$
C_m	pitching-moment coefficient, $\frac{M_Y}{qS\bar{c}}$
C_n	yawing-moment coefficient, $\frac{M_Z}{qSb}$
C_Y	lateral-force coefficient, $\frac{F_Y}{qS}$
$\bar{c}$	wing mean aerodynamic chord, ft
F_D	drag force, lb
F_L	lift force, lb
F_Y	side force, lb
f	frequency of the oscillation, cps
I_X	moment of inertia about X-axis, slug-ft^2

I_Z	moment of inertia about Z-axis, slug-ft^2
k	reduced-frequency parameter, $\omega b/2V$
M_X	rolling moment, ft-lb
M_Y	pitching moment, ft-lb
M_Z	yawing moment, ft-lb
P	period of oscillation, sec
p	rolling velocity, radians/sec
$\dot{p}$	rolling acceleration, radians/sec^2
r	yawing velocity, radians/sec
$\dot{r}$	yawing acceleration, radians/sec^2
q	dynamic pressure, $\rho V^2/2$, lb/sq ft
S	wing area, sq ft
$T_{1/2}$	time to damp to one-half amplitude, sec
V	free-stream velocity, ft/sec
v	velocity component along the Y-axis, ft/sec
X,Y,Z	coordinate body axes
α	angle of attack, deg
$\dot{\alpha}$	rate of change with angle of attack, radians/sec
β	angle of sideslip, $\sin^{-1}\frac{v}{V}$, deg
$\dot{\beta}$	rate of change with angle of sideslip, radians/sec
$\Delta C_Y, \Delta C_n, \Delta C_l$	incremental force and moment coefficients
δ_a	aileron deflection (elevons deflected differentially for aileron control), deg
δ_e	elevator deflection (elevons deflected together for elevator control), deg

δ_r rudder deflection, deg

ρ air density, slugs/cu ft

C_{l_β} effective-dihedral parameter, $\left(\frac{\Delta C_l}{\Delta \beta}\right)_{\beta=\pm 5^\circ}$

C_{n_β} directional-stability parameter, $\left(\frac{\Delta C_n}{\Delta \beta}\right)_{\beta=\pm 5^\circ}$

C_{Y_β} side-force parameter, $\left(\frac{\Delta C_Y}{\Delta \beta}\right)_{\beta=\pm 5^\circ}$

$$C_{l_r} = \frac{\partial C_l}{\partial\left(\frac{rb}{2V}\right)} \qquad C_{n_r} = \frac{\partial C_n}{\partial\left(\frac{rb}{2V}\right)} \qquad C_{Y_r} = \frac{\partial C_Y}{\partial\left(\frac{rb}{2V}\right)}$$

$$C_{l_p} = \frac{\partial C_l}{\partial\left(\frac{pb}{2V}\right)} \qquad C_{n_p} = \frac{\partial C_n}{\partial\left(\frac{pb}{2V}\right)} \qquad C_{Y_p} = \frac{\partial C_Y}{\partial\left(\frac{pb}{2V}\right)}$$

$$C_{l_{\dot\beta}} = \frac{\partial C_l}{\partial\left(\frac{\dot\beta b}{2V}\right)} \qquad C_{n_{\dot\beta}} = \frac{\partial C_n}{\partial\left(\frac{\dot\beta b}{2V}\right)} \qquad C_{Y_{\dot\beta}} = \frac{\partial C_Y}{\partial\left(\frac{\dot\beta b}{2V}\right)}$$

$$C_{l_{\dot r}} = \frac{\partial C_l}{\partial\left(\frac{\dot r b^2}{4V^2}\right)} \qquad C_{n_{\dot r}} = \frac{\partial C_n}{\partial\left(\frac{\dot r b^2}{4V^2}\right)} \qquad C_{Y_{\dot r}} = \frac{\partial C_Y}{\partial\left(\frac{\dot r b^2}{4V^2}\right)}$$

$$C_{l_{\dot p}} = \frac{\partial C_l}{\partial\left(\frac{\dot p b^2}{4V^2}\right)} \qquad C_{n_{\dot p}} = \frac{\partial C_n}{\partial\left(\frac{\dot p b^2}{4V^2}\right)} \qquad C_{Y_{\dot p}} = \frac{\partial C_Y}{\partial\left(\frac{\dot p b^2}{4V^2}\right)}$$

In the present investigation the term "out-of-phase derivative" refers to any one of the stability derivatives that are based on the components of the forces and moments 90° out of phase with the angle of roll, yaw, or sideslip. The term "in-phase derivative" refers to any one of the oscillatory derivatives that are based on the components of the forces and moments in phase with the angle of roll, yaw, or sideslip produced in the oscillatory tests. The oscillatory derivatives of the

present investigation were measured in the following combinations:

$$\left.\begin{aligned} &C_{l_p} + C_{l_{\dot{\beta}}} \sin \alpha \\ &C_{n_p} + C_{n_{\dot{\beta}}} \sin \alpha \\ &C_{Y_p} + C_{Y_{\dot{\beta}}} \sin \alpha \end{aligned}\right\} \text{Out-of-phase rolling derivatives}$$

$$\left.\begin{aligned} &C_{l_\beta} \sin \alpha - k^2 C_{l_{\dot{p}}} \\ &C_{n_\beta} \sin \alpha - k^2 C_{n_{\dot{p}}} \\ &C_{Y_\beta} \sin \alpha - k^2 C_{Y_{\dot{p}}} \end{aligned}\right\} \text{In-phase rolling derivatives}$$

$$\left.\begin{aligned} &C_{l_r} - C_{l_{\dot{\beta}}} \cos \alpha \\ &C_{n_r} - C_{n_{\dot{\beta}}} \cos \alpha \\ &C_{Y_r} - C_{Y_{\dot{\beta}}} \cos \alpha \end{aligned}\right\} \text{Out-of-phase yawing derivatives}$$

$$\left.\begin{aligned} &C_{l_\beta} \cos \alpha + k^2 C_{l_{\dot{r}}} \\ &C_{n_\beta} \cos \alpha + k^2 C_{n_{\dot{r}}} \\ &C_{Y_\beta} \cos \alpha + k^2 C_{Y_{\dot{r}}} \end{aligned}\right\} \text{In-phase yawing derivatives}$$

APPARATUS AND TEST TECHNIQUE

Model

A three-view drawing of the model is shown in figure 2 and a photograph of the model flying in the Langley full-scale tunnel is shown in figure 3. Table I gives the geometric characteristics of the model. Elevons consisting of plain flaps extending rearward from the trailing edges of the top and bottom surfaces of the wing were used for elevator

and aileron control, and outwardly deflecting surfaces located at the wing tips were used for rudder control.

Test Equipment and Setup

Static and dynamic force tests were conducted with the apparatus and testing technique described in reference 5. The flight investigation was conducted in the test section of the Langley full-scale tunnel with the test setup illustrated in figure 4. The flight-test technique and equipment are described in detail in reference 6.

TESTS

Flight Tests

Flight tests were made to study the stability and control characteristics of the model over an angle-of-attack range from about 20° to 40°. A series of flight tests was made at an angle of attack of about 29° to determine the effect of center-of-gravity position on the longitudinal characteristics of the model.

All flights were made with coordinated aileron and rudder control. The control deflections used for most of the flight tests were $\delta_a = \pm 8°$, $\delta_r = \pm 15°$, and $\delta_e = \pm 7°$.

The model behavior during flight was observed by the pitch pilot located at the side of the test section and by the roll and yaw pilot located in the rear of the test section. The results obtained in the flight tests were primarily in the form of qualitative ratings of flight behavior based on pilot opinion. The motion-picture records obtained in the tests were used to verify and correlate the ratings for the different flight conditions.

Force Tests

Force tests were made to determine the static longitudinal and lateral stability and control characteristics of the model over an angle-of-attack range from 0° to 60° for the model with fuselage on and off. Static longitudinal stability and control tests were made over the angle-of-attack range for elevator deflections of 0°, -10°, and -20°. Force tests were made at various angles of attack to determine the static lateral stability and control characteristics of the model with and without the vertical tails over a sideslip range of ±20°.

Rotary oscillation tests were made to determine the dynamic lateral stability derivatives of the model. The tests were made for values of the reduced-frequency parameter k of 0.09 and 0.18.

All the tests were made at a dynamic pressure of about 3.97 pounds per square foot, which corresponds to an airspeed of about 58 feet per second at standard sea-level conditions and to a test Reynolds number of 1.46×10^6, based on the mean aerodynamic chord of 3.95 feet.

FORCE-TEST RESULTS AND DISCUSSION

Static Longitudinal Stability and Control Characteristics

The effect of elevator deflection on the longitudinal characteristics of the basic model and the model with fuselage off are shown in figures 5(a) and (b), respectively. The data show that both configurations were generally stable up to an angle of attack of 30°. The data also show that with the addition of the fuselage the model became less stable, had a lower lift-curve slope, and a lower value of maximum lift coefficient which is probably a result of a decrease in lift over the rear of the model.

Static Lateral Stability Characteristics

The variation of the coefficients C_Y, C_n, and C_l with sideslip angle for various angles of attack is shown in figures 6 and 7 for the basic model and the model with fuselage off, respectively. The lateral stability parameters C_{Y_β}, C_{n_β}, and C_{l_β} determined from figures 6 and 7 for angles of sideslip of $\pm 5^\circ$ are presented in figure 8. Since most of the data have a nonlinear variation with sideslip angle, the lateral stability parameters presented in figure 8 should be used only to give an indication of the trends in the lateral stability characteristics of the model over the angle-of-attack range of the investigation.

The data of figure 8 show that there were large variations in the values of the directional stability parameter C_{n_β} for the basic model with the model being directionally unstable $\left(-C_{n_\beta}\right)$ from angles of attack of about 18° to 25° and above an angle of attack of about 40°. The data of figure 8 are not identical to those of reference 2. The differences can probably be accounted for by the fact that different models were used in the investigations and, also, that in this angle-of-attack range there were large variations of yawing moment with angle of sideslip for

both models. The data of figure 8 show that with the fuselage off there was much less variation of C_{n_β} with angle of attack and the model was directionally stable up to an angle of attack of about 36°. Both the basic and fuselage-off configurations had positive effective dihedral $\left(-C_{l_\beta}\right)$ over most of the angle-of-attack range with the fuselage-off configuration having the greatest values of $-C_{l_\beta}$ up to an angle of attack of about 30°.

The aileron-control-effectiveness data of figure 9 show that there was a gradual decrease in rolling moment with increase in angle of attack. The basic model had favorable yawing moments due to aileron deflection up to a higher angle of attack than the model with the fuselage off. The data of figure 10 show that the yawing moments produced by deflecting the rudder decreased gradually with increasing angle of attack and became adverse at angles of attack above about 45°.

L
1
8
0
7

Oscillatory Lateral Stability Derivatives

The variation of the in-phase derivatives with angle of attack for both model configurations is shown in figure 11. Also presented in this figure for the purpose of comparison are static values (k = 0) of the lateral stability parameters taken from figure 8. These data show that there are large differences between the static and oscillation test results particularly at angles of attack from about 20° to 40°. Apparently these differences are due to large changes in the flow between the static and dynamic conditions.

The variation of the out-of-phase derivatives with angle of attack for both configurations is shown in figure 12. The data show that both configurations had small values of positive damping in roll $-\left(C_{l_p} + C_{l_{\dot\beta}} \sin \alpha\right)$ and damping in yaw $-\left(C_{n_r} - C_{n_{\dot\beta}} \cos \alpha\right)$ in the low angle-of-attack range. With increasing angle of attack the damping in roll increased while the damping in yaw decreased and became unstable. It should be noted that there are abrupt changes in all of the derivatives from angles of attack of about 25° to 50°.

FLIGHT-TEST RESULTS AND DISCUSSION

A motion-picture film supplement covering the flight tests has been prepared and is available on loan. A request card form and a description of the film will be found at the back of this paper, on the page immediately preceding the abstract page.

Longitudinal Stability and Control

During the investigation made to study the longitudinal stability and control characteristics of the model, artificial damping in roll and a ventral tail were used in order to minimize any effects lateral motions might have on the longitudinal behavior.

As part of the investigation of longitudinal stability and control a series of flights was made with the basic model at an angle of attack of 29° to determine the effect of the center-of-gravity location. Static tests indicated that at this angle of attack the model was neutrally stable at a center-of-gravity position of about 33 percent of the mean aerodynamic chord. With positive stability (center of gravity ahead of the 33-percent mean-aerodynamic-chord location) the model flew smoothly and the pilot had no trouble in controlling it. With neutral stability, the model could still be flown smoothly but slightly more attention to longitudinal control was required than for the flights in which the model had positive stability. Flights could be made with a static margin of -5 percent (center of gravity at 0.38$\bar{c}$) as long as the model did not experience a large disturbance, but the pilot had to give constant attention to longitudinal control to prevent a divergence in pitch.

In addition to the studies of the center-of-gravity range made at an angle of attack of 29°, flights were made at angles of attack from about 20° to 40° with a center-of-gravity position (0.29$\bar{c}$) that gave good static longitudinal stability at an angle of attack of 29°. The model was flown up to an angle of attack of about 40°. Although the force-test data of figure 5 indicate a region of static longitudinal instability between angles of attack of 30° and 35°, this instability did not appear to be particularly troublesome to the pilot, apparently because it occurred over such a small angle-of-attack range and there was adequate stability on each side of the instability range.

Lateral Stability and Control

No artificial roll damping.- With no artifical roll damping, the lateral stability and control characteristics of the model were considered to be poor from angles of attack of about 20° to 30° and flights were impossible above an angle of attack of 30° because of poor damping and control. The model had a rather large amplitude, erratic Dutch roll oscillation which made it very difficult to control and required the constant attention of the pilot in an effort to keep it flying. The erratic nature of the model motions can probably be explained by the data of figure 11 which show large variations in the forces and moments determined during static and dynamic test conditions. The oscillation appeared to be an almost pure rolling motion about the body axis, which is a characteristic of models of this shape which have large values of

I_Z/I_X and C_{l_β}/C_{n_β}. In these tests the flights usually terminated because the model would slide off to the left or right out of control. Although it appeared that control effectiveness was involved, the force-test data of figures 9 and 10 indicate that there should have been sufficient control effectiveness to insure satisfactory lateral control up to an angle of attack of about 40°. The fact that in the flight tests the lateral control seemed to be weak was probably a result of the large amplitude oscillation which introduced forces and moments that the controls could not handle.

The results of the lateral-stability calculations to determine the damping and period characteristics of the model are presented in figure 13. The results are in fair agreement with the flight-test results up to an angle of attack of about 30°, in that they show about neutral stability for the Dutch roll oscillation. However, above an angle of attack of 30° the calculations indicate the Dutch roll oscillation was damped, whereas the flight tests indicated a lightly damped or neutrally stable Dutch roll oscillation. This difference between the calculations and the flight-test results is probably attributed to the fact that the derivatives used in the calculations were measured for an amplitude of ±5°, whereas the measured amplitude of the oscillations of the flight-test model were as high as ±18°. Previous studies have shown that differences in amplitude could produce large changes in the magnitude of the derivatives involved and, therefore, would likely have a considerable effect on calculated Dutch roll damping characteristics.

Artificial roll damping added.- The addition of artificial rate roll damping to improve the stability of the Dutch roll oscillation greatly improved the lateral characteristics of the model so that flights could be made up to an angle of attack of about 40°. The model was easy to fly at the lower angles of attack but flights were difficult to maintain at the higher angles of attack because there was some deterioration of stability and control with increasing angle of attack. These flight-test results are in good agreement with the data of figure 14 which show that increasing $-C_{l_p}$ at an angle of attack of 30° greatly improves the damping of the Dutch roll oscillation.

SUMMARY OF RESULTS

The results of the investigation are as follows:

1. The longitudinal flight characteristics were considered to be generally satisfactory over the angle-of-attack range (20° to 40°) of the investigation.

2. Because of low damping of the Dutch roll oscillation, the lateral stability and control characteristics were considered to be poor throughout the angle-of-attack range (20° to 30°) where flights were possible without artificial damping. Artificial damping in roll greatly improved the lateral characteristics so that flights could be made up to an angle of attack of about 40°.

Langley Research Center,
National Aeronautics and Space Administration,
Langley Air Force Base, Va., October 30, 1961.

REFERENCES

1. Penland, Jim A., and Armstrong, William O.: Preliminary Aerodynamic Data Pertinent to Manned Satellite Reentry Configurations. NACA RM L58E13a, 1958.

2. Paulson, John W.: Low-Speed Static Stability Characteristics of Two Configurations Suitable for Lifting Reentry From Satellite Orbit. NASA MEMO 10-22-58L, 1958.

3. Hassell, James L., Jr.: Investigation of the Low-Subsonic Stability and Control Characteristics of a 1/3-Scale Free-Flying Model of a Lifting-Body Reentry Configuration. NASA TM X-297, 1960.

4. Paulson, John W., Shanks, Robert E., and Johnson, Joseph L.: Low-Speed Flight Characteristics of Reentry Vehicles of the Glide-Landing Type. NASA TM X-331, 1960.

5. Hewes, Donald E.: Low-Subsonic Measurements of the Static and Oscillatory Lateral Stability Derivatives of a Sweptback-Wing Airplane Configuration at Angles of Attack From -10° to 90°. NASA MEMO 5-20-59L, 1959.

6. Paulson, John W., and Shanks, Robert E.: Investigation of Low-Subsonic Flight Characteristics of a Model of a Hypersonic Boost-Glide Configuration Having a 78° Delta Wing. NASA TN D-894, 1961. (Supersedes NASA TM X-201.)

TABLE I.- GEOMETRIC CHARACTERISTICS OF THE MODEL

Airfoil section	Flat plate
Area (includes cutouts), sq ft	9.80
Span, ft	2.75
Aspect ratio	0.77
Root chord, ft	5.78
Tip chord, ft	1.00
Mean aerodynamic chord, ft	3.95
Sweepback of wing leading edge, deg	75
Dihedral, deg	0

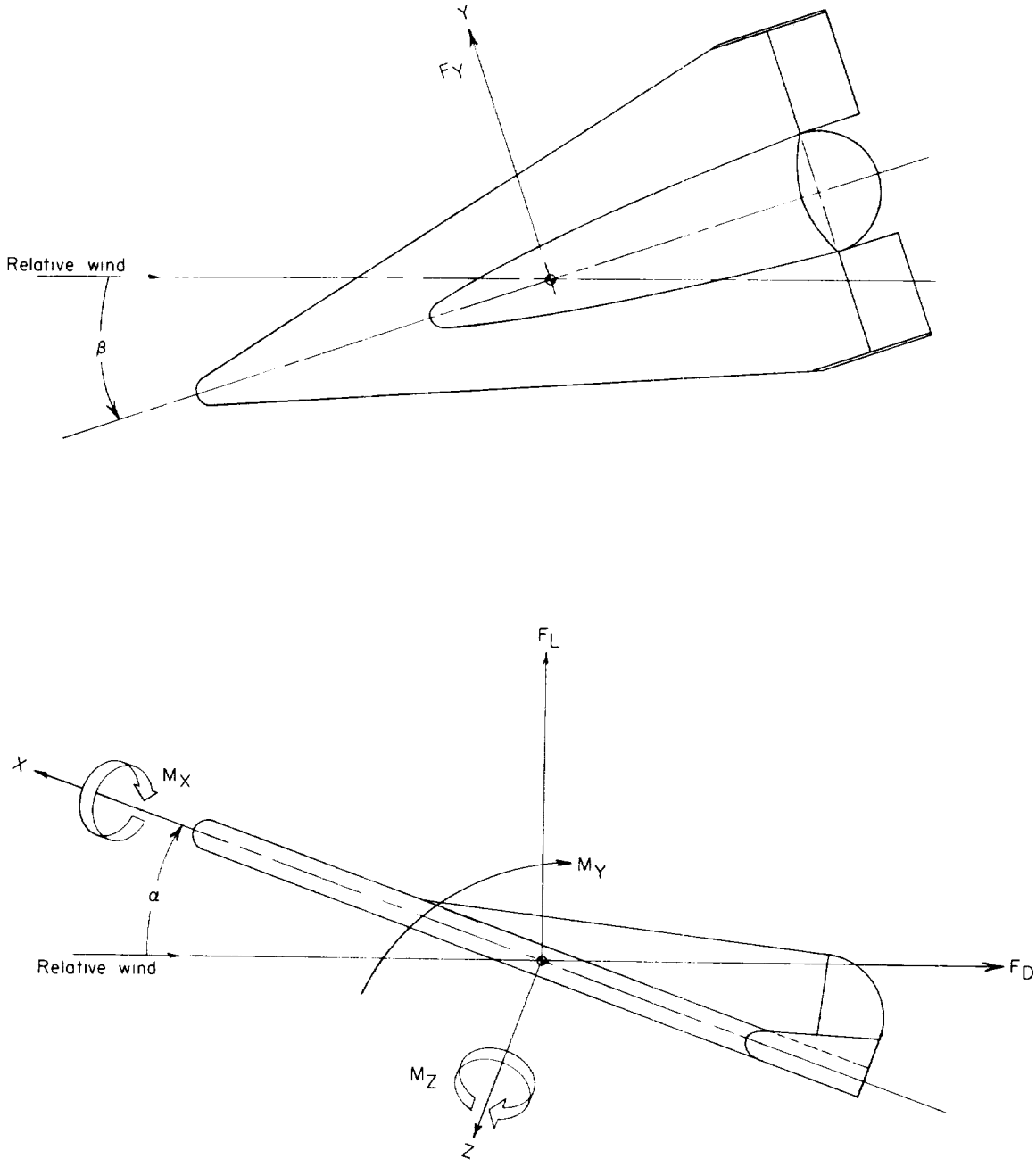

Figure 1.- Sketch of axis system showing positive direction of forces, moments, and angles.

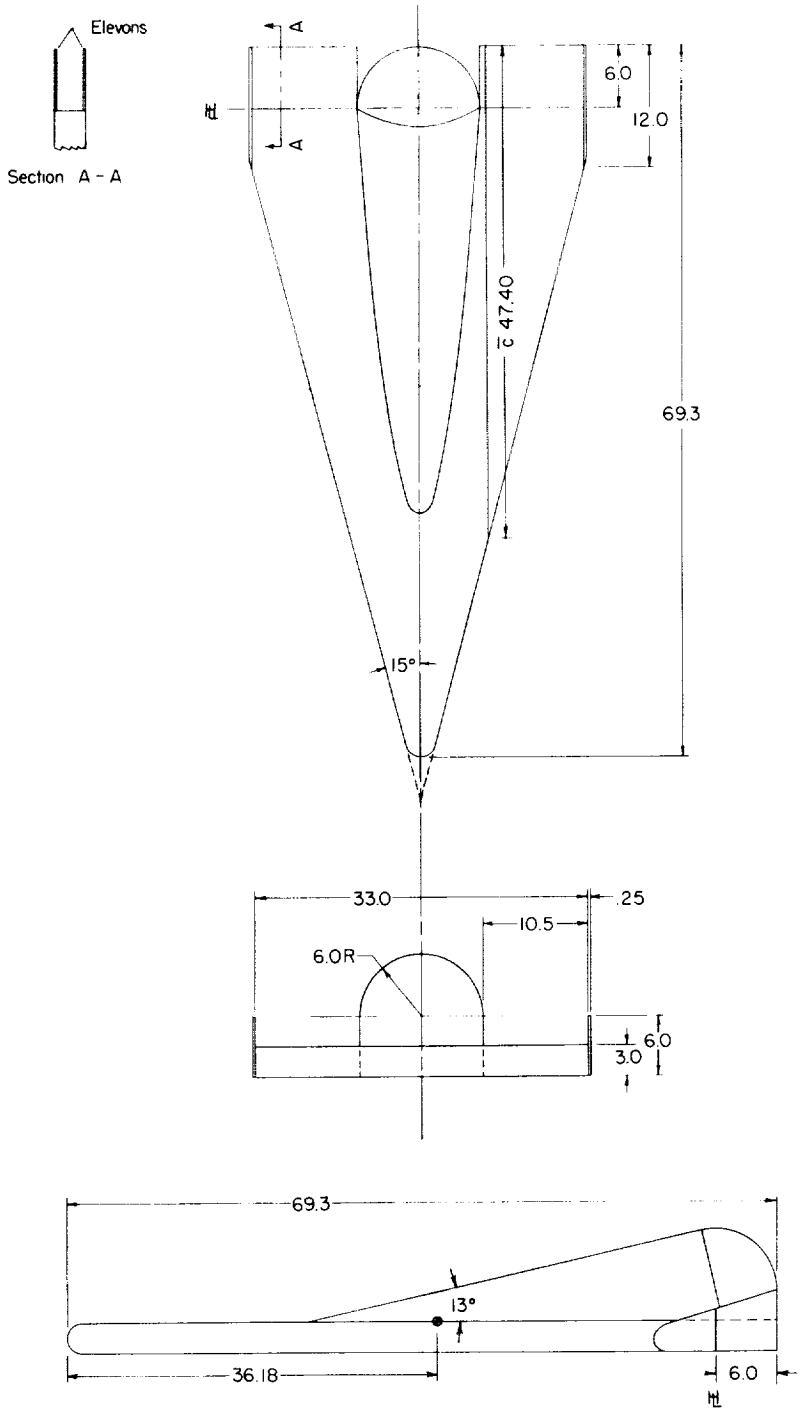

Figure 2.- Three-view drawing of model used in the investigation. All dimensions are in inches.

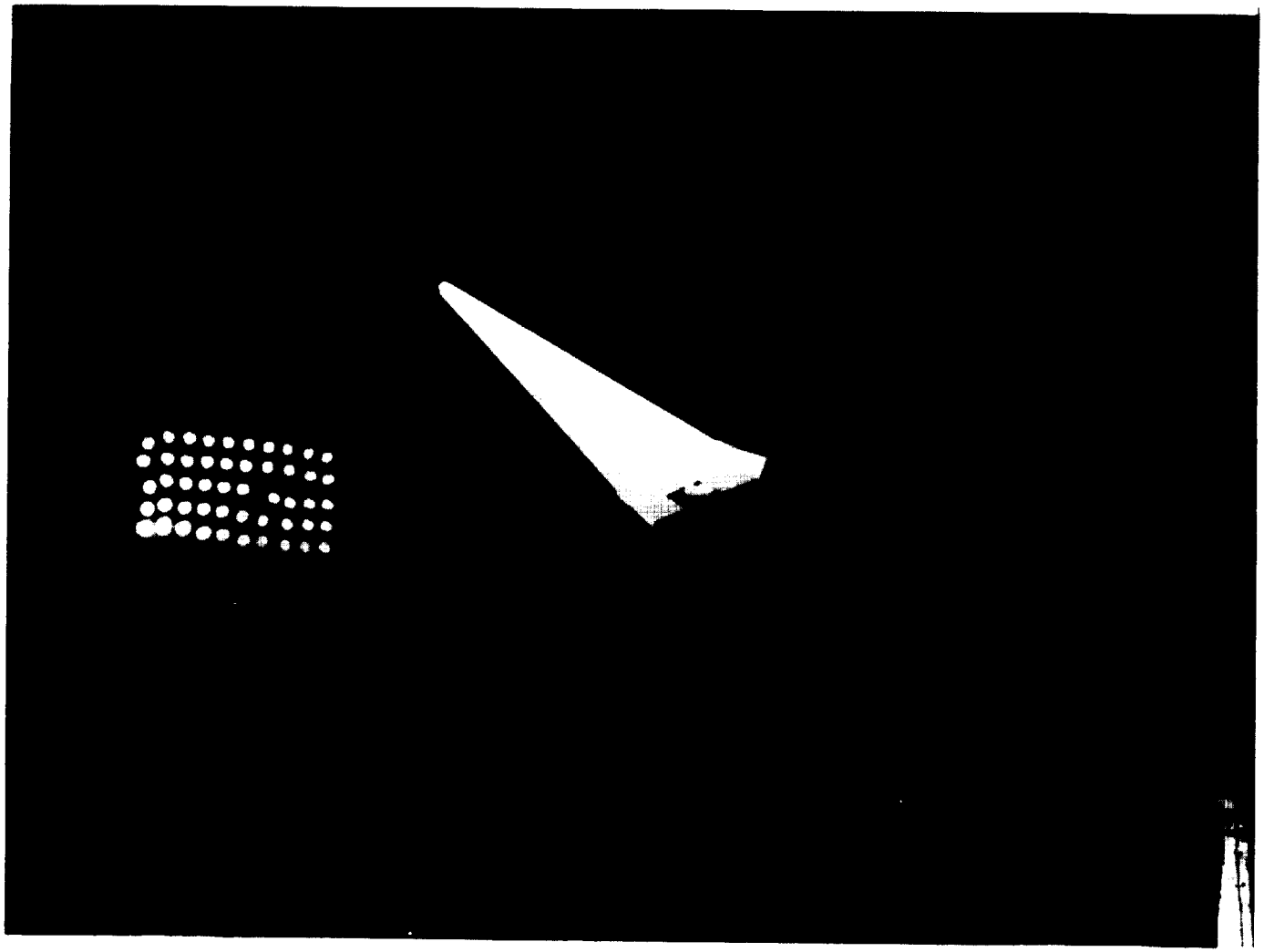

L-59-2140

Figure 3.- Model flying in Langley full-scale tunnel.

15

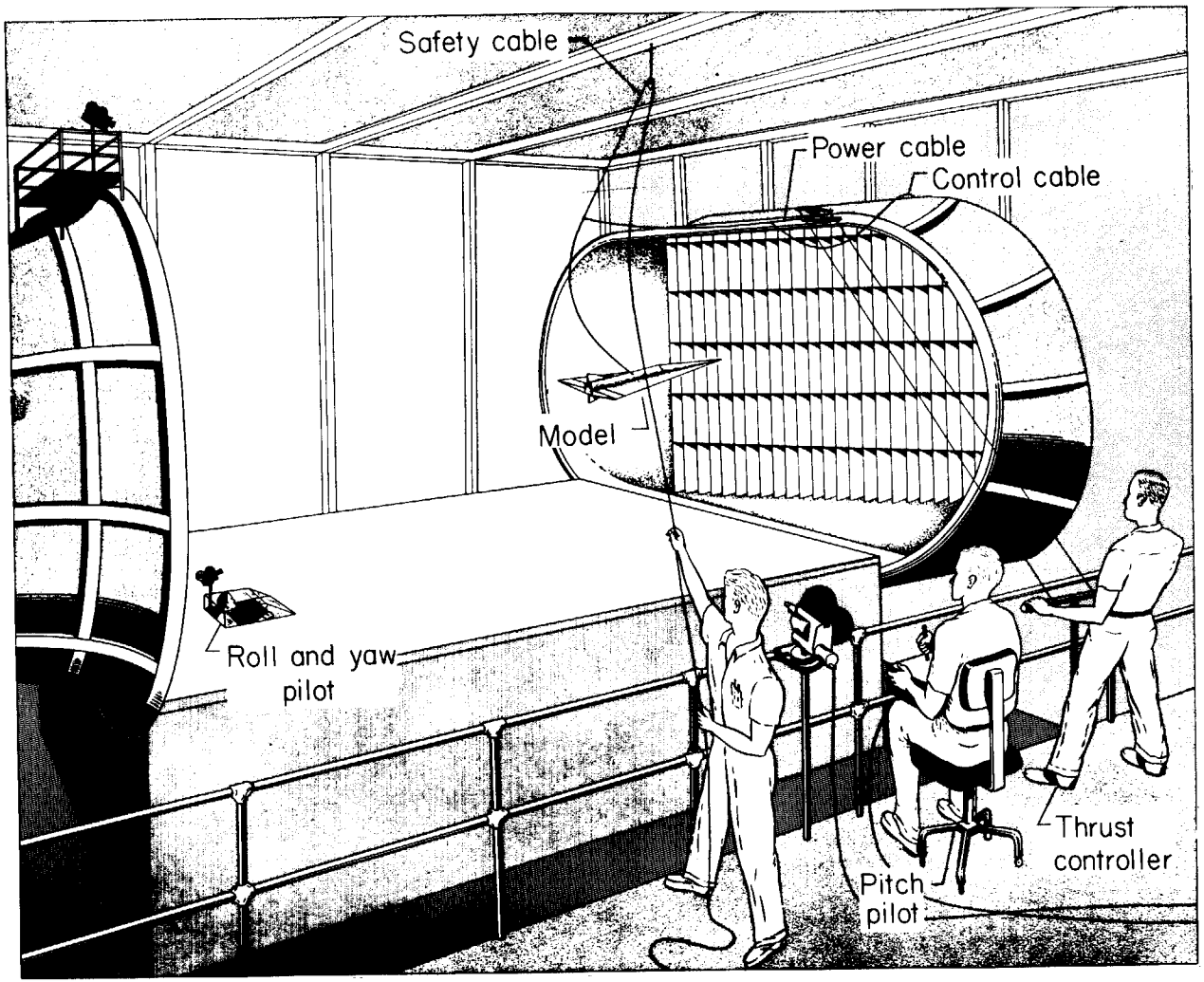

Figure 4.- Sketch of test setup in Langley full-scale tunnel.

L-1807

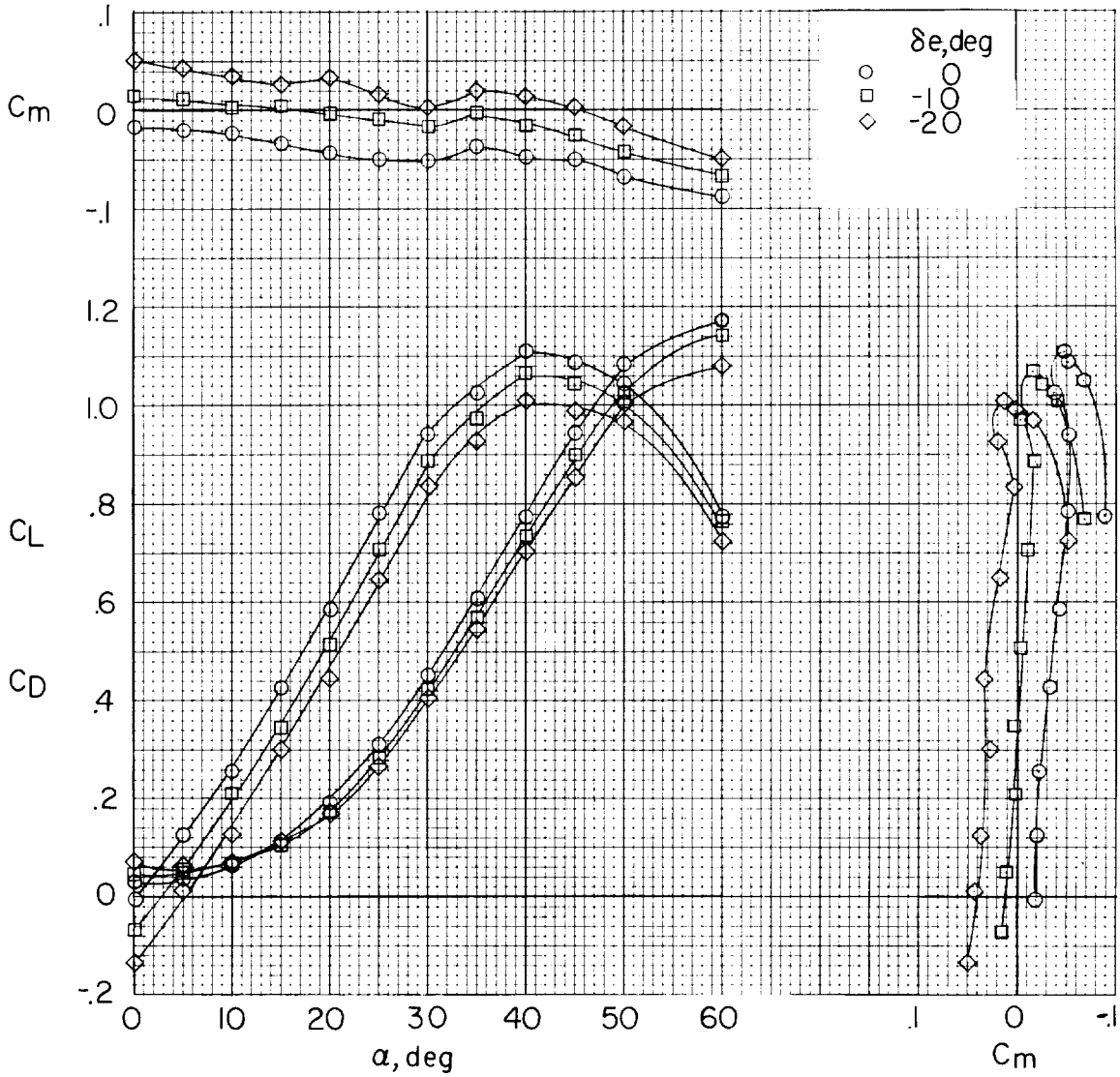

(a) Fuselage on.

Figure 5.- Longitudinal characteristics of the configuration.

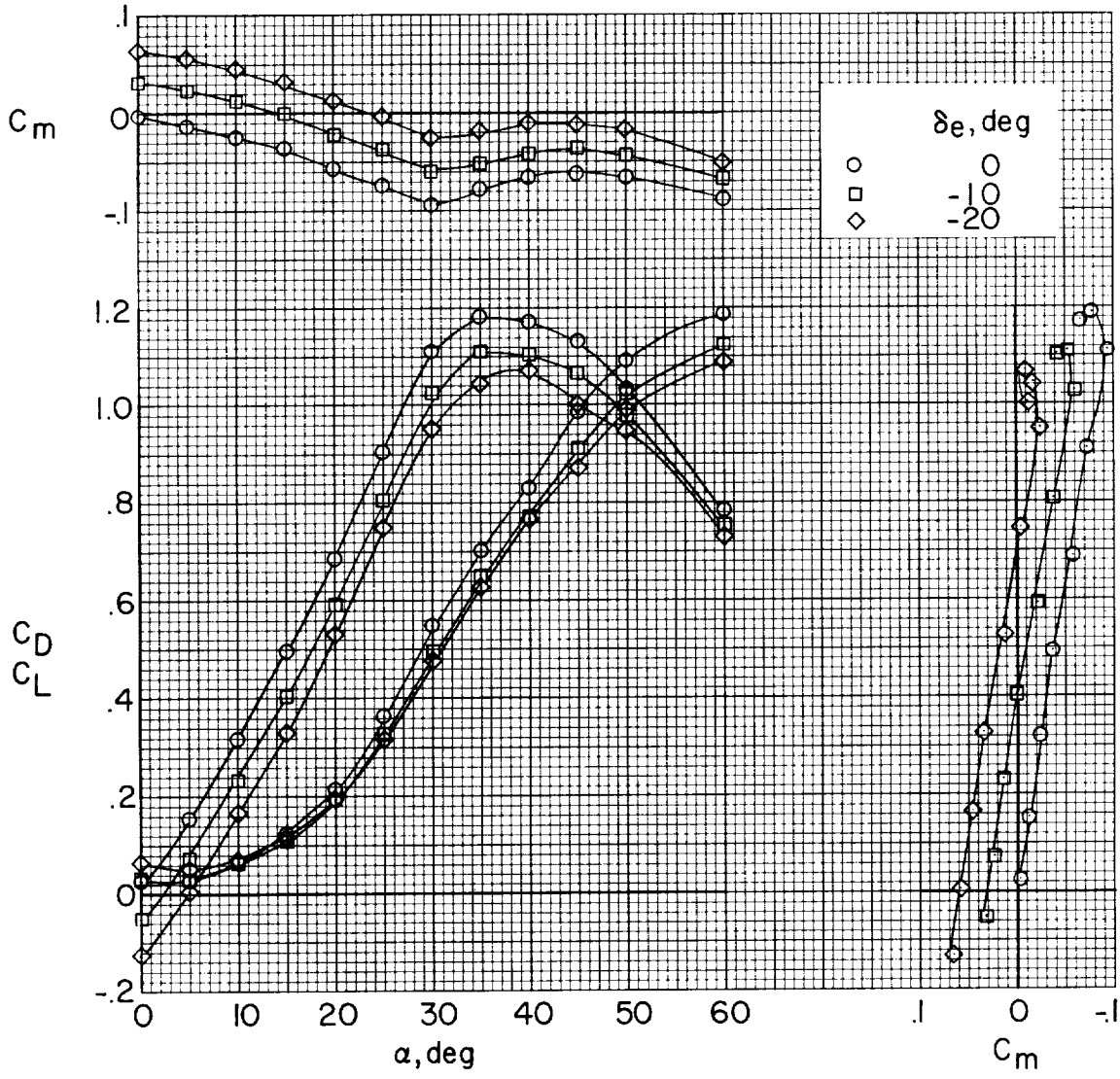

(b) Fuselage off.

Figure 5.- Concluded.

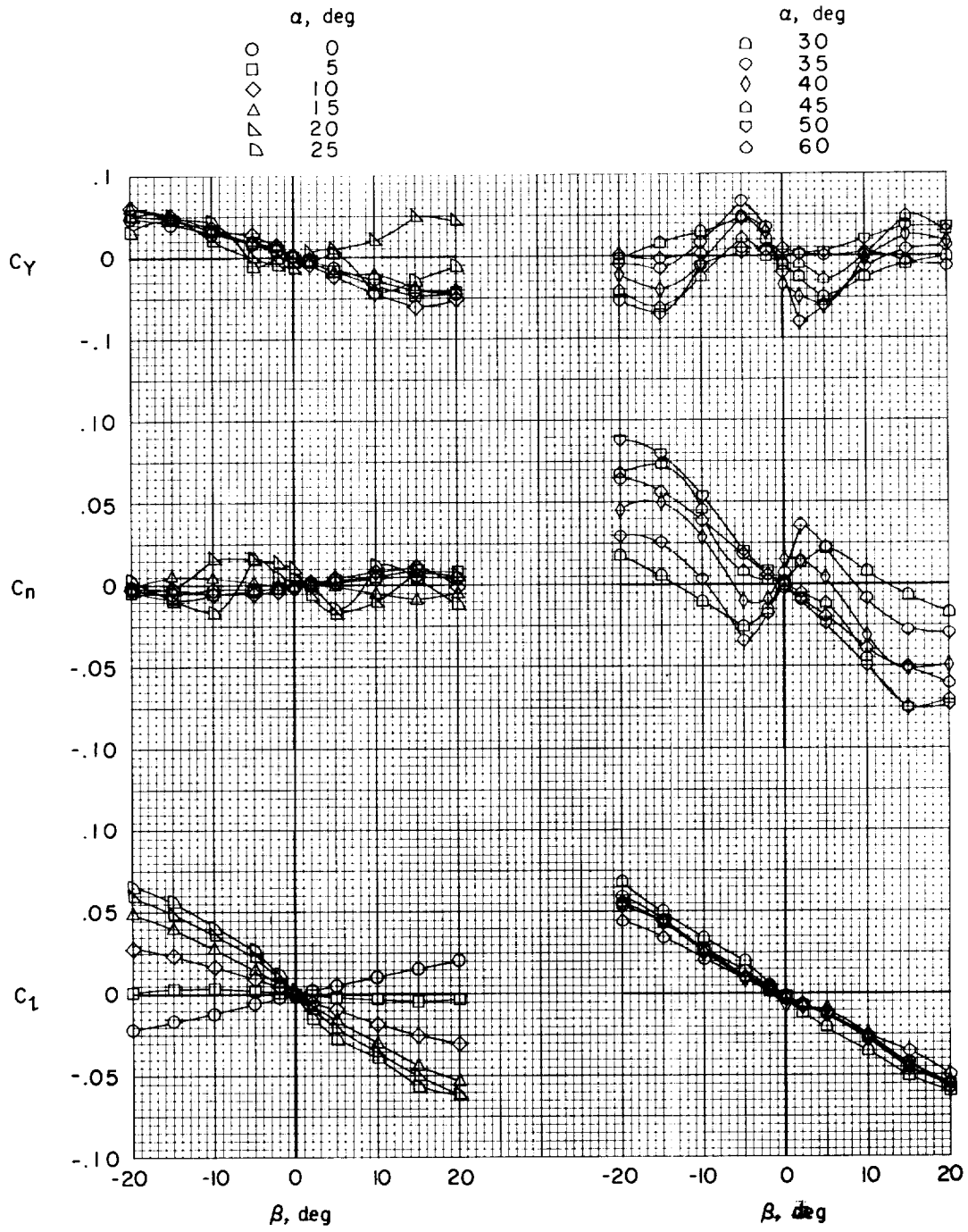

(a) Vertical tails off.

Figure 6.- Variation of static lateral stability characteristics with angle of sideslip for the model with fuselage on. $\delta_e = -10^\circ$.

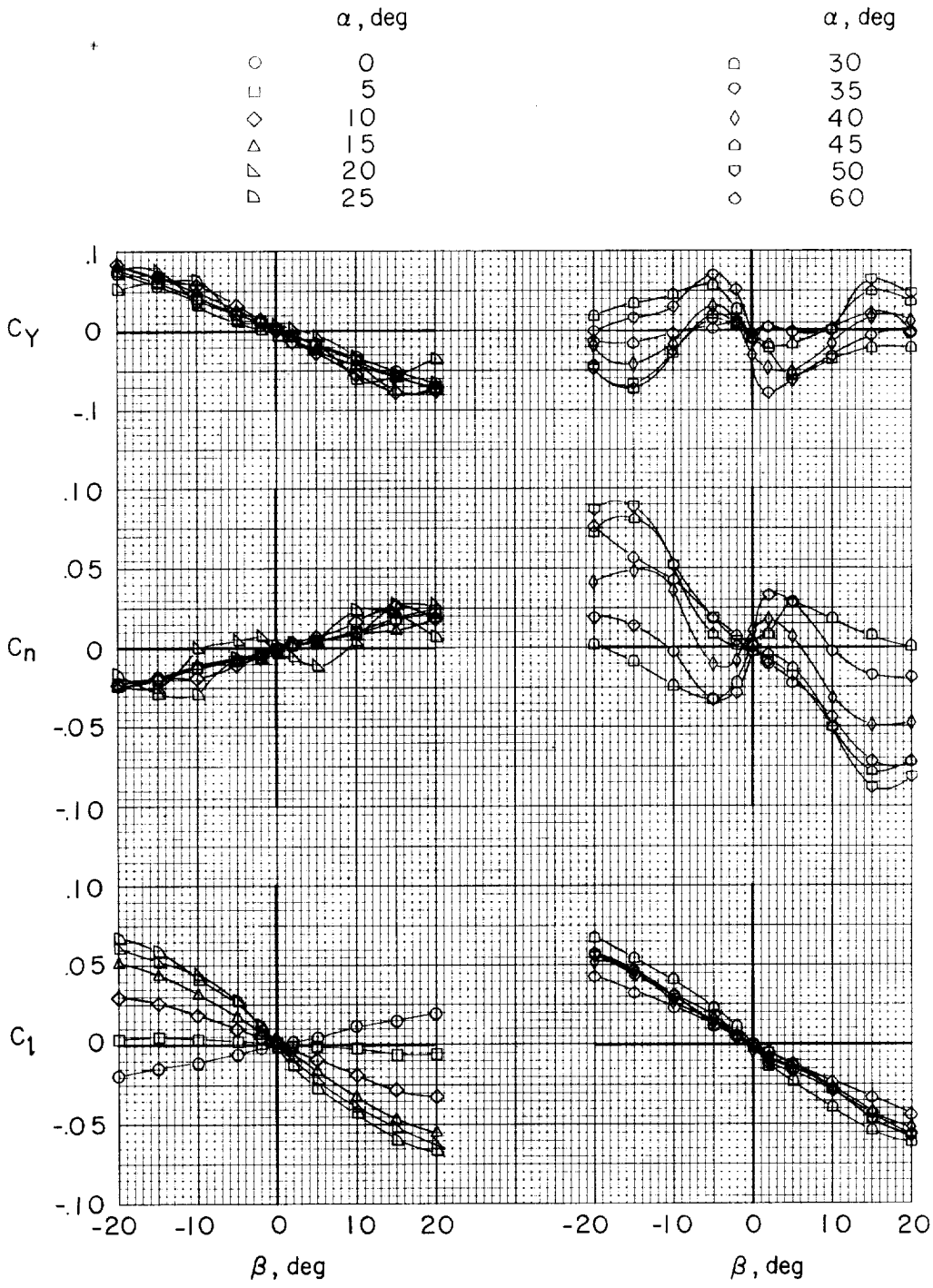

(b) Vertical tails on.

Figure 6.- Concluded.

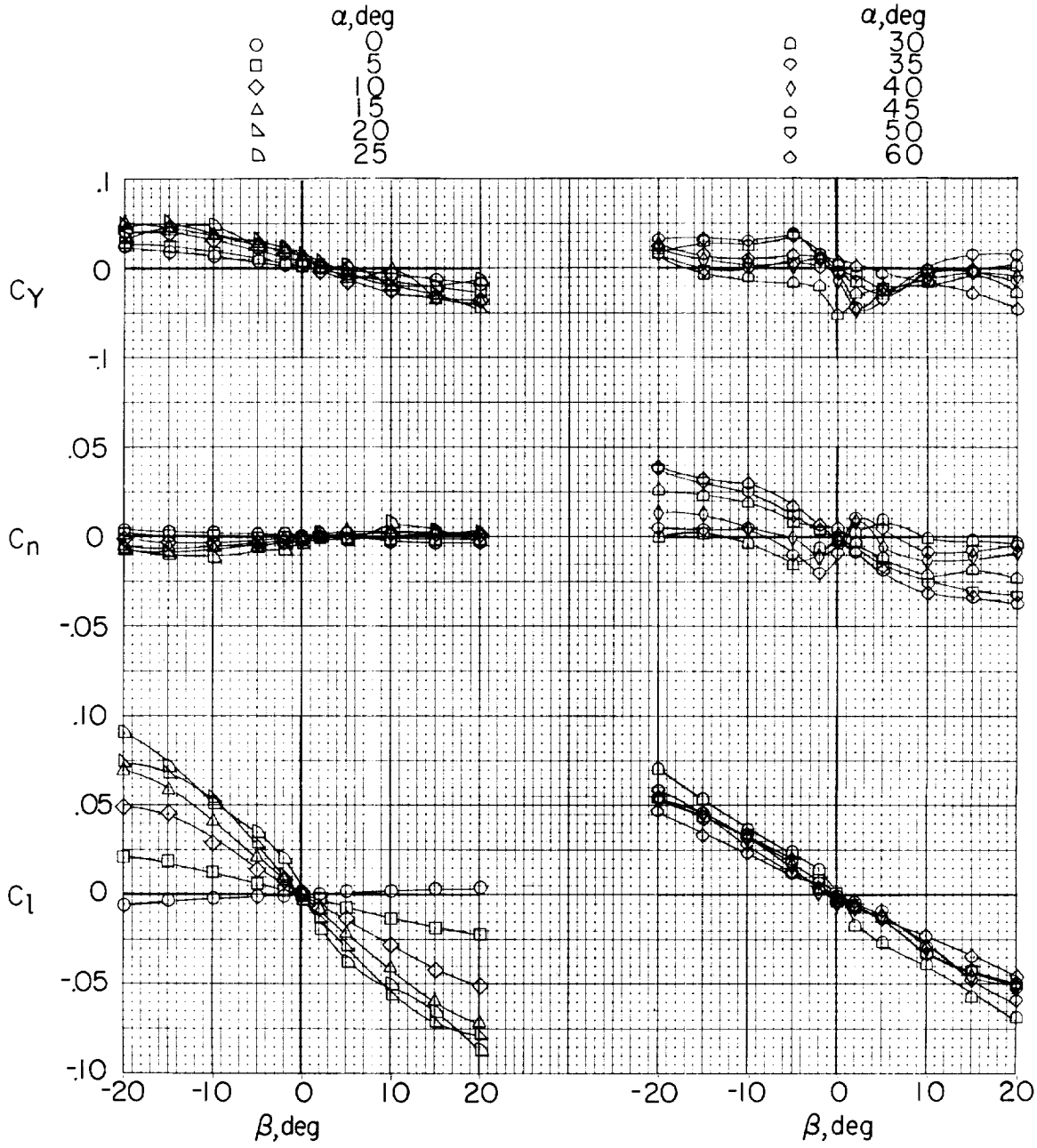

(a) Vertical tails off.

Figure 7.- Variation of static lateral stability characteristics with angle of sideslip for the model with fuselage off. $\delta_e = -10^o$.

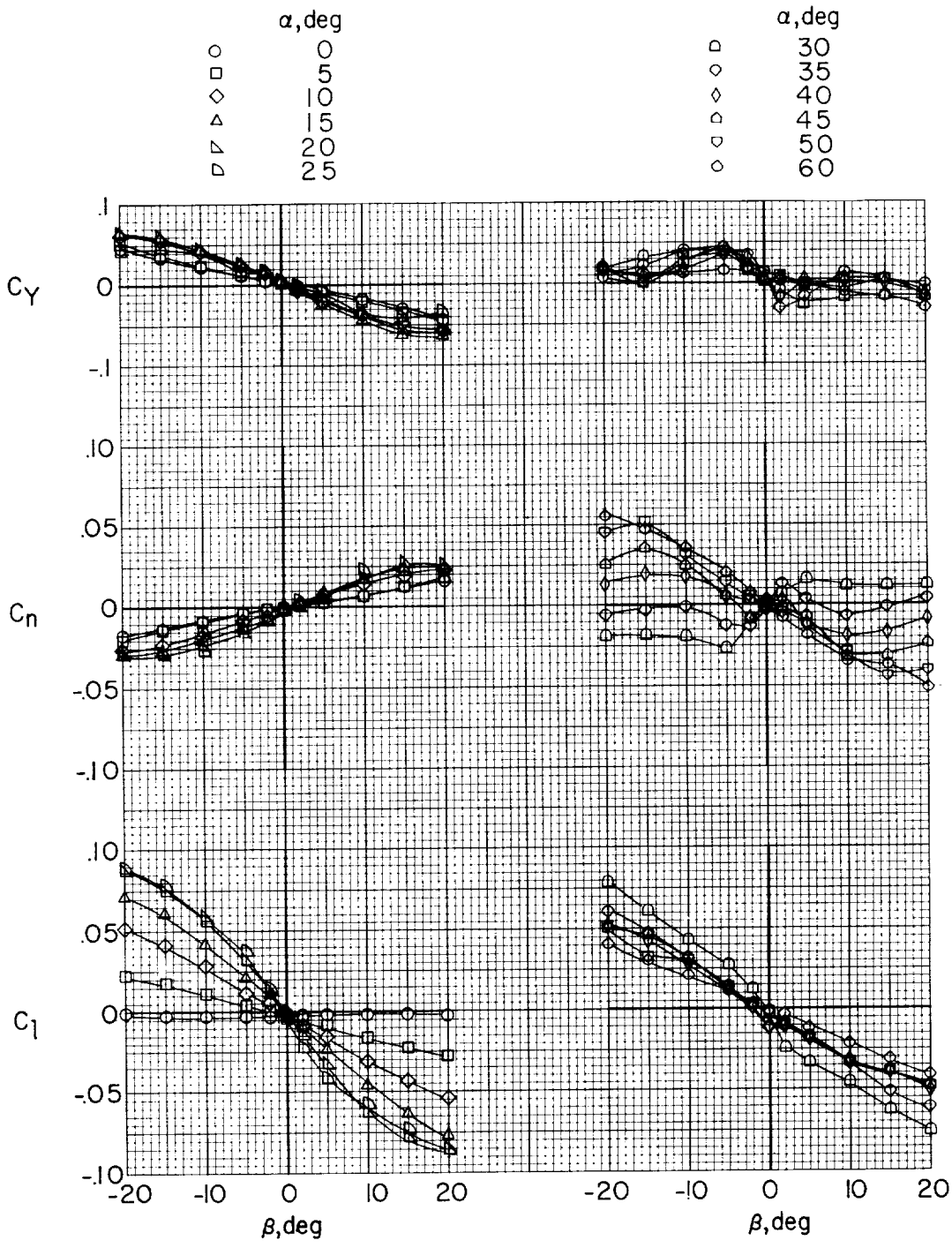

(b) Vertical tails on.

Figure 7.- Concluded.

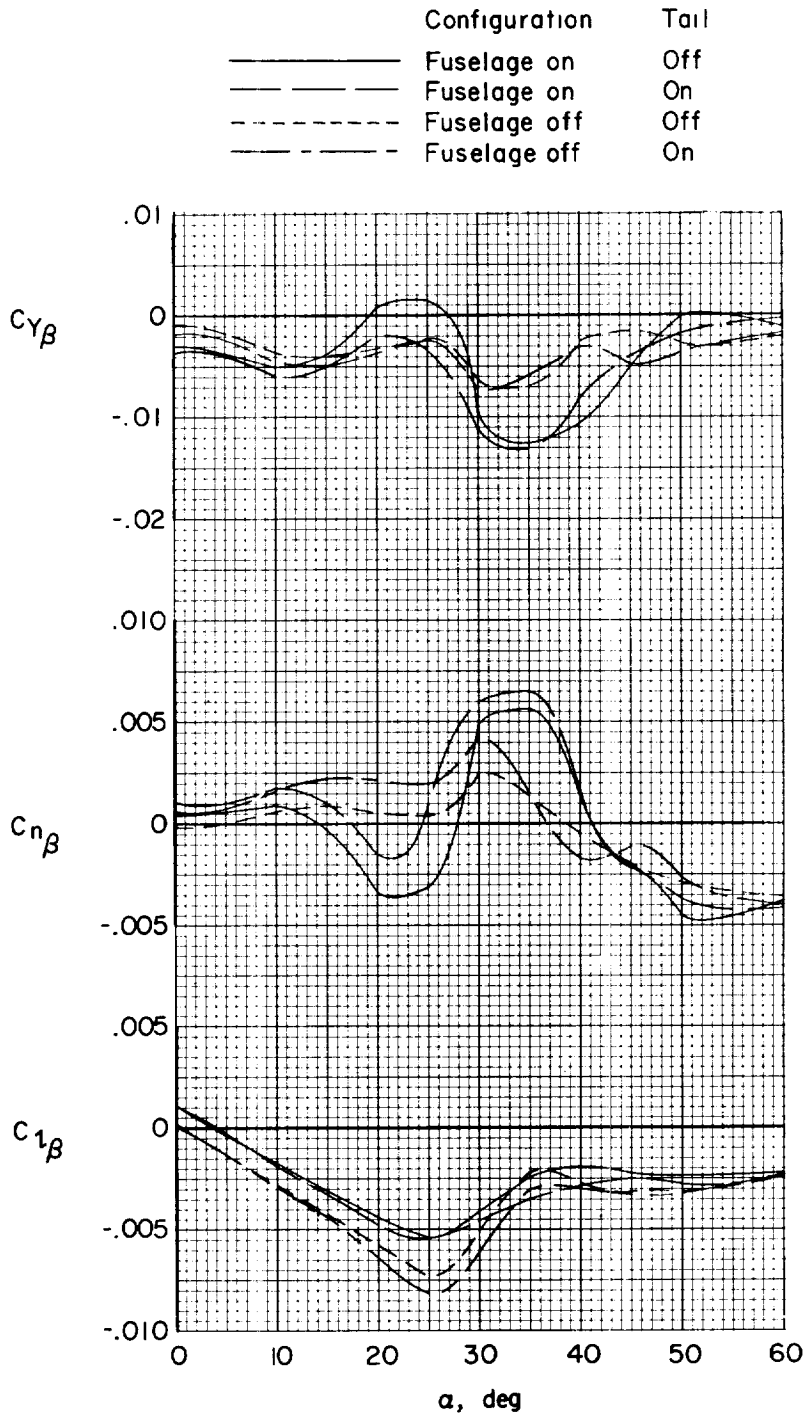

Figure 8.- Comparison of the sideslip derivatives of the model with fuselage on and with fuselage off. $\delta_e = -10^\circ$.

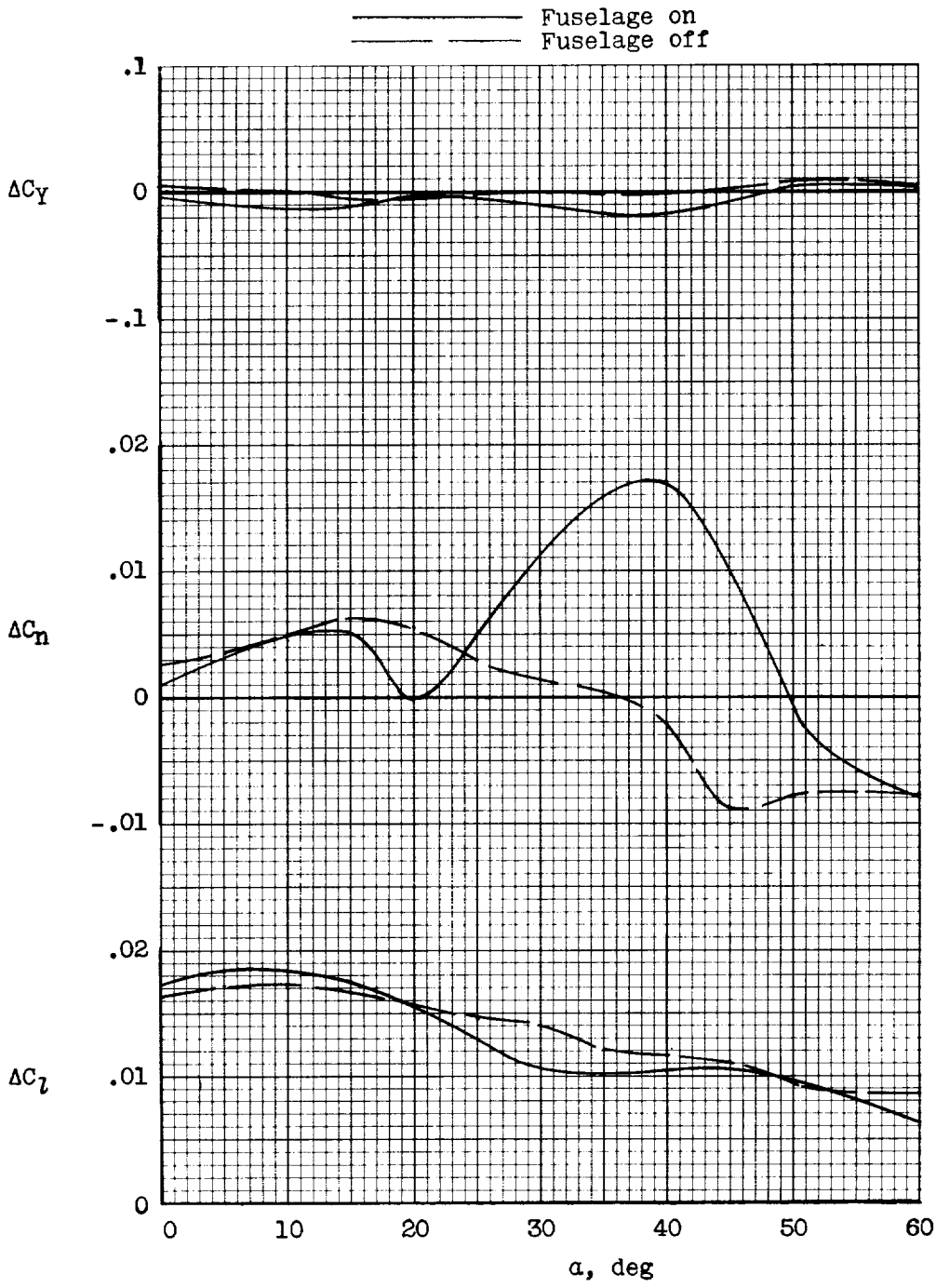

L-1807

Figure 9.- Incremental lateral control coefficients due to differential deflection of elevons (trailing edge 0° on left surface and trailing edge 20° upward on right surface).

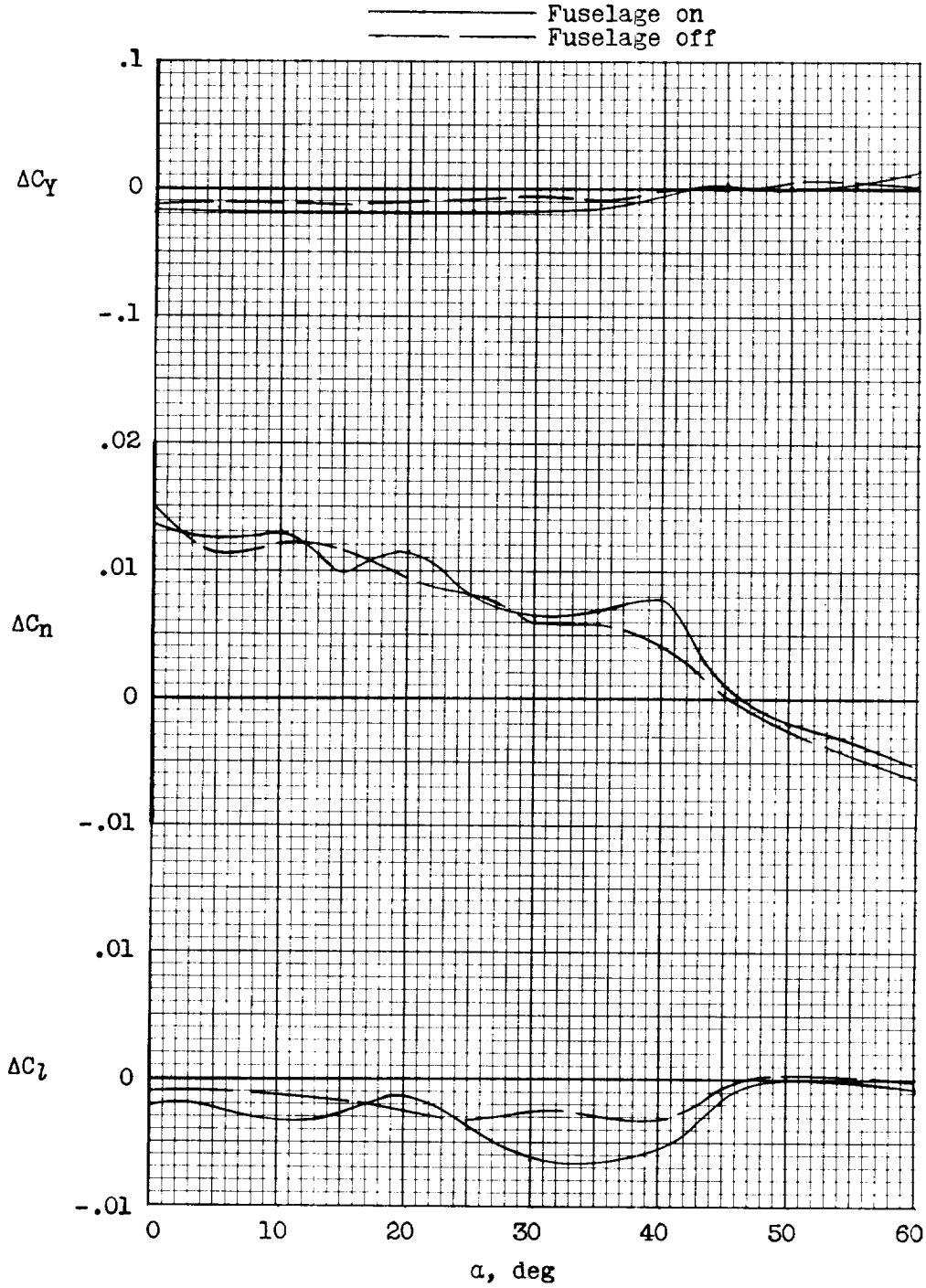

Figure 10.- Increments of lateral force and moment coefficients produced by deflecting the rudder -20°. δ_e = -10°.

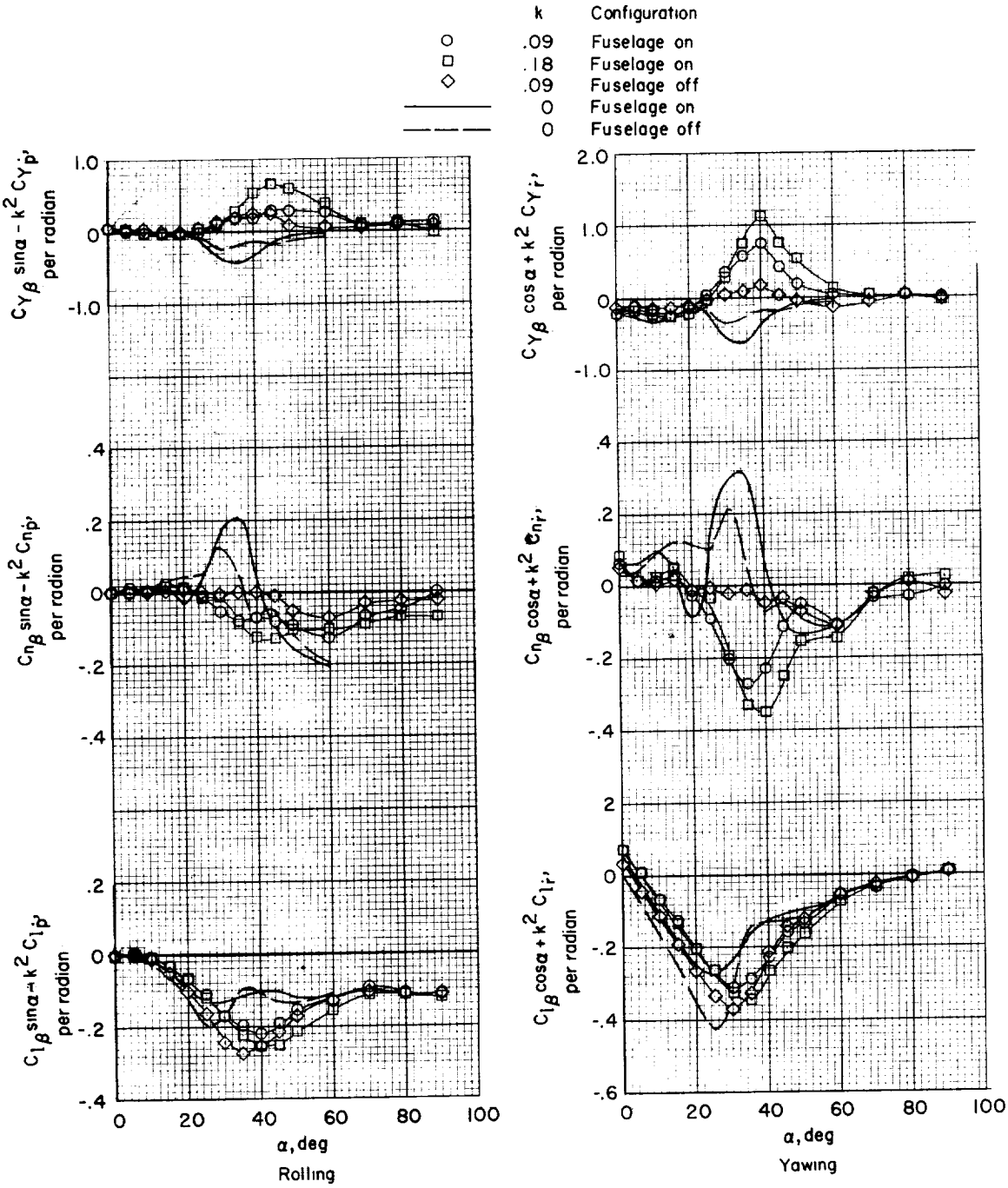

L-1807

Figure 11.- Variation of the in-phase derivatives with angle of attack. $\delta_e = -10^\circ$.

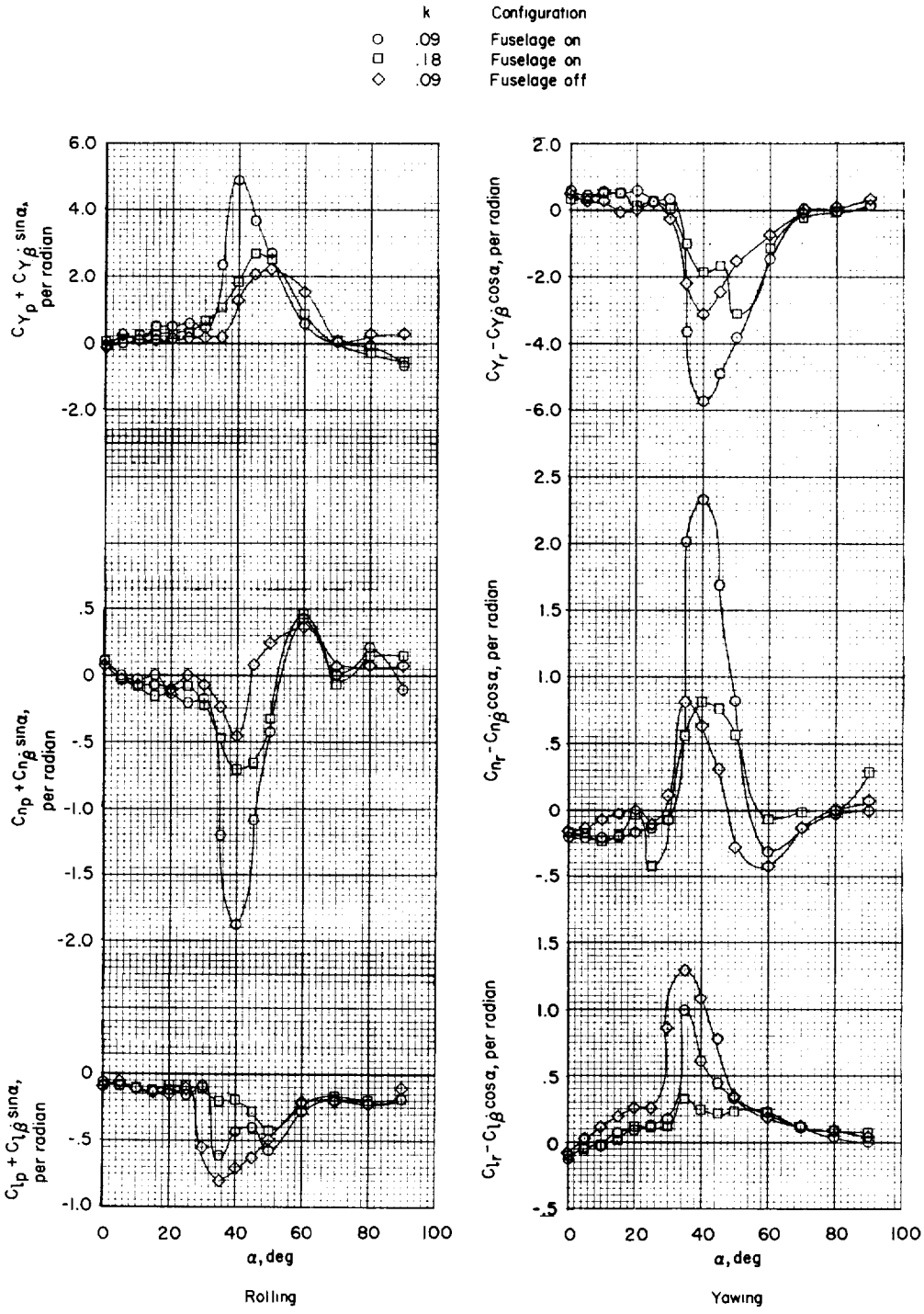

Figure 12.- Variation of the out-of-phase derivatives with angle of attack. $\delta_e = -10^\circ$.

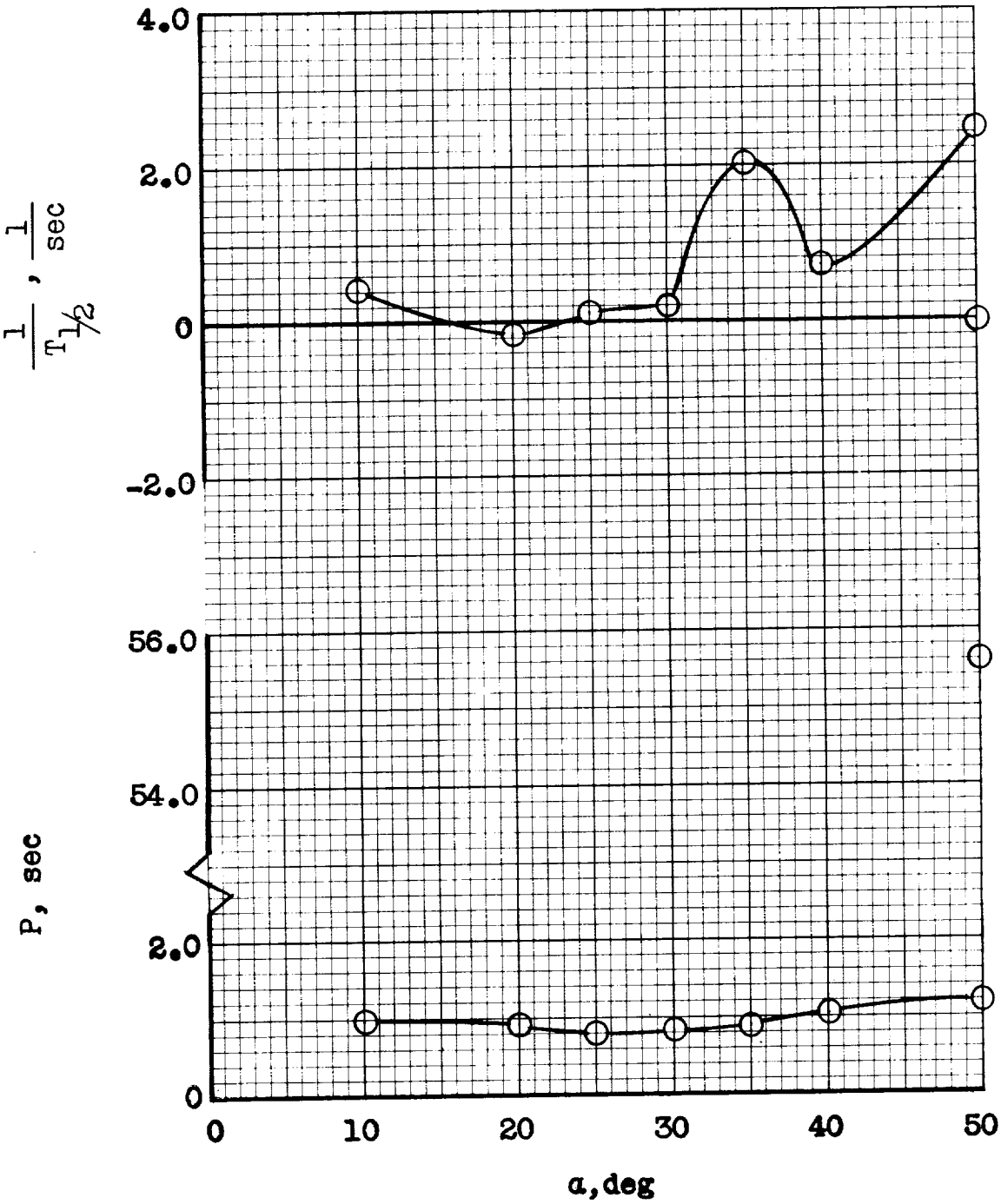

Figure 13.- Calculated period and time to damp to half-amplitude of the Dutch roll oscillation for the model with fuselage on.

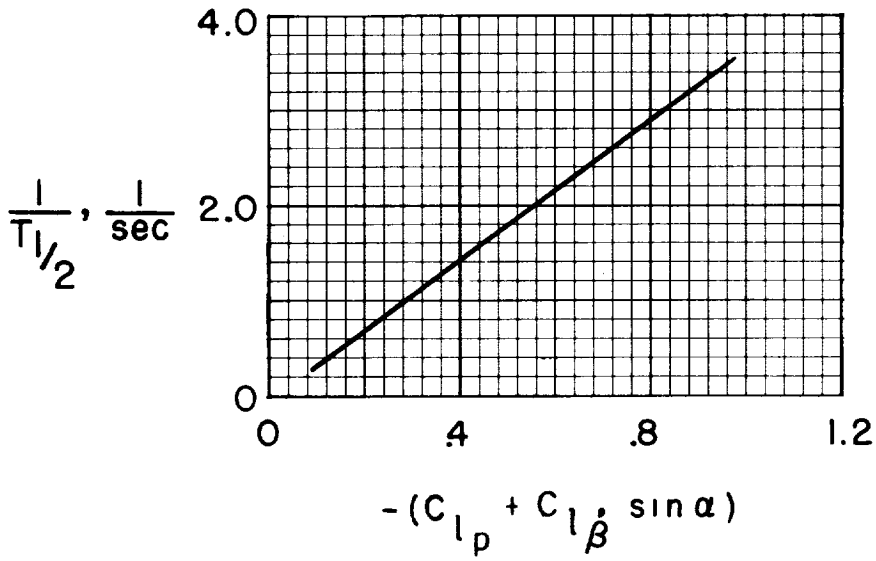

Figure 14.- Effect of variation of C_{l_p} on the calculated damping of the Dutch roll oscillation. $\alpha = 30^\circ$.